Nanoscience and Nanotechnology 2013, 3(5): 130-134
DOI: 10.5923/j.nn.20130305.04

X-ray Diffraction and UV-Visible Characterizations of α-Fe_2O_3 Nanoparticles Annealed at Different Temperature

P. Mallick[1,*], B. N. Dash[2]

[1]Department of Physics, North Orissa University, Baripada 757003, Odisha, India
[2]Department of Physics, Salipur College, Salipur 754103, Odisha, India

Abstract Effect of annealing on the microstructure, optical absorption properties of hematite (α-Fe_2O_3) nanoparticles were studied. Crystallite size of α-Fe_2O_3 increased from ~ 34 to 44 nm with increasing annealing temperature from 500 to 700℃. Strain in the sample decreased with increasing annealing temperature. UV-visible characterization indicated the existence of both direct and indirect band gap in the samples. The samples annealed at all temperatures showed the direct band gap at ~ 2.67 eV. However, the indirect band gap increased from 1.6 to 1.94 eV when the annealing temperature increased from 500 to 600℃ and remained almost same for sample annealed at 700℃. The observed values of optical band gaps were in close agreement with the reported values. Our results indicated that the thermal annealing would give rise to well crystalline α-Fe_2O_3 nanoparticles with reduced strain.

Keywords Iron Oxide, Nanoparticle, Annealing, Microstructure, Band Gap

1. Introduction

In recent years, research on transition metal oxide (TMOs) nanoparticles has attracted much attention for their potential technological applications. Iron oxide is one of the most important transition metal oxide. Iron oxide exhibits different phases such as FeO, α-Fe_2O_3, γ-Fe_2O_3, β-Fe_2O_3 and Fe_3O_4. Hematite (α-Fe_2O_3) is the most stable iron oxide under ambient conditions. It is a low cost non-toxic environment friendly material easily available in nature[1]. It shows n-type semiconducting properties with band gap = 2.2eV which lies in the visible region[2]. α-Fe_2O_3 exhibits rhombohedrally centred hexagonal structure of the corundum type with a close packed oxygen lattice in which two-thirds of the octahedral sited are occupied by Fe (III) ions[3]. α-Fe_2O_3 exhibits canted antiferromagnetic (weakly ferromagnetic) at room temperature, antiferromagnetic below the Morin transition temperature of 250 K and paramagnetic above its Néel temperature of 948 K[4]. α-Fe_2O_3 shows wide varieties of applications such as light-induced water splitting[5], catalysis[6], gas sensors[7], solar cells[8], field emission devices[9], magnetic recording [10] drug delivery[11], tissue repair engineering[12], magnetic resonance imaging[13], pigments[14], lithium-ion batteries[10] and spin electronic devices[15].

Several methods have been adopted for the synthesis of nanoparticles of α-Fe_2O_3 such as sol–gel[16], chemical precipitation[17], forced hydrolysis[18, 19], hydrothermal [20, 21], sonochemical[22], solution combustion[23], high-energy ball milling[24] etc. Among the above method, some of them are very expensive and required large time for the synthesis of final product. It is therefore essential that the synthesis route would facilitate for large scale synthesis of nanoparticles of α-Fe_2O_3 in cost effective and easier manner.

In this paper, we report the synthesis of α-Fe_2O_3 nanoparticles using a simple low cost chemical route and studied the effect of thermal annealing on their the microstructure and optical absorption properties.

2. Experimental Methods

α-Fe_2O_3 nanoparticles were synthesized by chemical route using iron nitrate ($Fe(NO_3)_3.9H_2O$) (MERCK, India) as starting material. In this procedure, homogeneous solutions of required amount of $Fe(NO_3)_3.9H_2O$ in distilled water was prepared with the help of magnetic stirrer. This solution was aged for 1 day and then dried at 100℃. Then the resultant product is calcined at 300℃ for 1 hour and then pressed into pellets. These pellets are annealed at 500, 600 and 700℃ for 1 hour in order to get α-Fe_2O_3 nanoparticles used in the present study.

The structural and microstructural evolutions of α-Fe_2O_3 nanoparticles were studied by X-ray diffraction with CuKα radiation using Bruker X-ray diffractometer (Model:

* Corresponding author:
pravanjan_phy@yahoo.co.in (P. Mallick)
Published online at http://journal.sapub.org/nn

D8 Advance). The optical absorption spectroscopy of α -Fe_2O_3 nanoparticles were performed using diffuse reflectance spectroscopy by a double beam UV-Visible spectrophotometer (Simadzu, UV-2450) with an integrating sphere assembly.

3. Results and Discussion

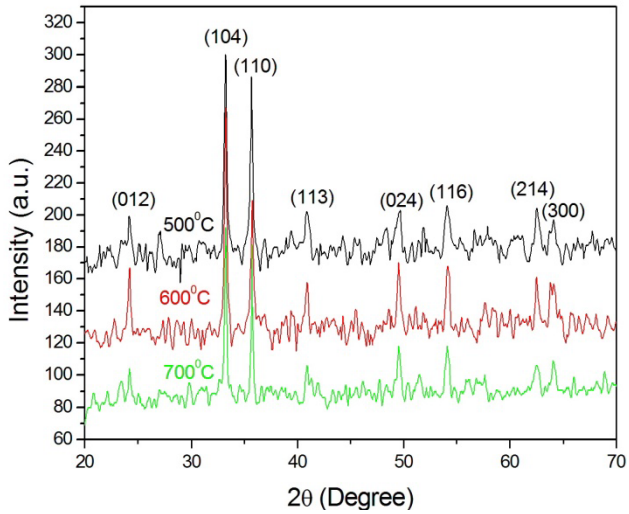

Figure 1. XRD pattern of α -Fe_2O_3 nanoparticle annealed at different temperature

Figure 1 shows the XRD pattern of Fe_2O_3 nanoparticle annealed at 500, 600 and 700℃. All peaks appeared in the XRD pattern are indexed to the hexagonal structure (space group: $R\bar{3}c$) of α -Fe_2O_3 and are well consistent with the JCPDS card (card no: 33-0664). In order to see the effect of annealing temperature on the microstructural properties we estimated the average crystallite size (D) and the strain (ε) present in α -Fe_2O_3nanoparticles from the full width at half maximum (FWHM) of the first major XRD peak using the following equations[25]:

$$D = \frac{0.94\lambda}{\beta \cos\theta} \quad (1)$$

and

$$\varepsilon = \frac{\beta \cos\theta}{4} \quad (2)$$

where β is the FWHM, θ is the Bragg angle and λ is the wavelength of Cu K α radiation. Figure 2 shows the variation of crystallite size and strain for α -Fe_2O_3 nanoparticle annealed at different temperature. Crystallite size increased from ~ 34 to 44 nm when annealing temperature increased from 500 to 700℃. Increase of crystallite size for α -Fe_2O_3 nanoparticles from ~ 18 to 54 nm was reported when the annealing temperature increased from 300 to 500℃[26]. So our samples contain relatively smaller crystallites even though we use higher annealing temperature. This behaviour may be reflected in the optical band gap of the sample which discussed later. The strain in our sample decreased with increasing annealing temperature. Our results indicated that the annealing is essential for synthesis of good crystalline stain free α -Fe_2O_3 nanoparticles.

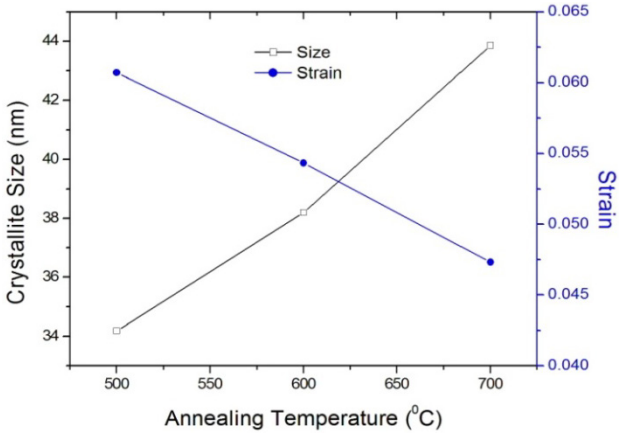

Figure 2. Variation of crystallite size and strain for α -Fe_2O_3 nanoparticle annealed at different temperature

Optical band gap of α -Fe_2O_3 nanoparticles annealed at different temperature were estimated by using UV-Visible absorption spectroscopy. Figure 3 shows the variation of absorption coefficient, α of α -Fe_2O_3 nanoparticles annealed at 500, 600 and 700℃ as a function of wavelength. The absorption intensity for all samples increased with decreasing wavelength due to nanocrystalline nature of the material[19]. It has reported that the absorption spectra of α -Fe_2O_3 nanoparticles in the entire wavelength can be divided into 4 regions: region I (250–400 nm), region II (400-600 nm), region III (600-780 nm) and region IV (750-900 nm) based on different transitions[27]. Since in our case, absorption coefficient was recorded in the wavelength range 200-800 nm, we do not have much information about the region IV. It is worthy to mention that the absorption coefficients of Fe_2O_3nanocrystals in the range of 600-900 nm are minor[28].The absorption bands appeared in region I are due to the ligand-to-metal charge-transfer (LMCT) transitions (direct transitions) with combined contributions from the Fe^{3+} ligand field transitions $^6A_1(^6S)$ to $^4T_1(^4P)$ at 290–310 nm, $^6A_1(^6S)$ to $^4E(^4D)$ and $^6A_1(^6S)$ to $^4T_1(^4D)$ at 360–380 nm[29, 30]. The absorption band in region II is associated with the double excitation processes $^6A_1(^6S)$+$^6A_1(^6S)$ to $^4T_1(^4G)$+$^4T_1(^4G)$ at 485–550 nm, and is most likely overlapped by the contributions of $^6A_1(^6S)$ to ^4E, $^4A_1(^4G)$ ligand field transitions at 430 and the charge-transfer band tail[28, 29, 31]. This inter-band transition is primarily responsible for the red colour of hematite. Region III corresponds to the $^6A_1(^6S)$ to $^4T_2(^4G)$ ligand field transition at about 640 nm[28, 31].

The optical band gap was extracted according to the following relation[32]:

$$\alpha = \frac{B(h\nu - E_g)^n}{h\nu} \quad (3)$$

where $h\nu$ is the incident photon energy, α is the absorption coefficient, B is a materials dependent constant and E_g is the optical band gap. The value of n depends

on the nature of transition. Depending on whether the transition is direct allowed, direct forbidden, indirect allowed or indirect forbidden, n takes the value 1/2, 3/2, 2 or 3 respectively[33]. The usual method of determining E_g involves plotting $(\alpha h\nu)^{1/n}$ vs. $h\nu$. By extrapolating the linear portion of the $(\alpha h\nu)^{1/n}$ vs. $h\nu$ plot to $\alpha = 0$, we can estimate the band gap from the absorption peak. Some reports indicated that α -Fe_2O_3 is an indirect band gap material[34, 35] and some other reported the existence of direct band gap in α -Fe_2O_3[36]. It has also been reported that α -Fe_2O_3 exhibits both direct band gap and indirect band gaps[1, 2, 37, 38]. The spin forbidden Fe^{3+} 3d $\rightarrow$ 3d excitation gives rise to indirect transition and the direct transition corresponds to the O^{2-} 2p $\rightarrow$ Fe^{3+} 3d charge transfer[39, 40]. We therefore investigated the occurrence of both direct and indirect transitions in our case by plotting $(\alpha h\nu)^{1/n}$ vs. $h\nu$ with n =1/2 (Fig. 4) and 2 (Fig. 5) respectively. The value of direct band gap for the sample annealed at all temperatures is ~ 2.67eV (Fig. 4). The observed values of direct band gaps in our case were in close agreement with the value (~ 2.65 eV) reported by Banerjee et al.[26]. The reported values of the indirect band gap for α -Fe_2O_3 were varied from 1.38 to 2.09 eV[1, 2, 34, 35, 37, 38, 41]. The values of indirect band gap obtained from Fig. 5 for different annealed samples are in good agreement with the reported values. Unlike direct band gap, the indirect band gap increased from 1.6 to 1.94 eV when the annealing temperature increased from 500 to 600 ℃. The sample annealed at 700 ℃ exhibits indirect band gap at 1.93 eV. Similar type of observation has been reported by Al-Kuhaili et al.[2]. These authors have shown that the indirect band gaps increased when heated substrate is used during deposition whereas the direct band gaps did not show any variation. Our results are in agreement with the reported results[2].

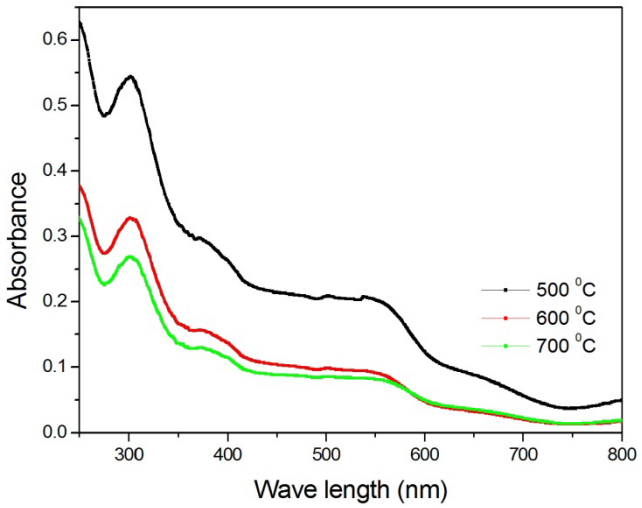

Figure 3. Variation of absorption coefficient of α -Fe_2O_3 nanoparticles annealed at 500, 600 and 700 ℃ with wavelength

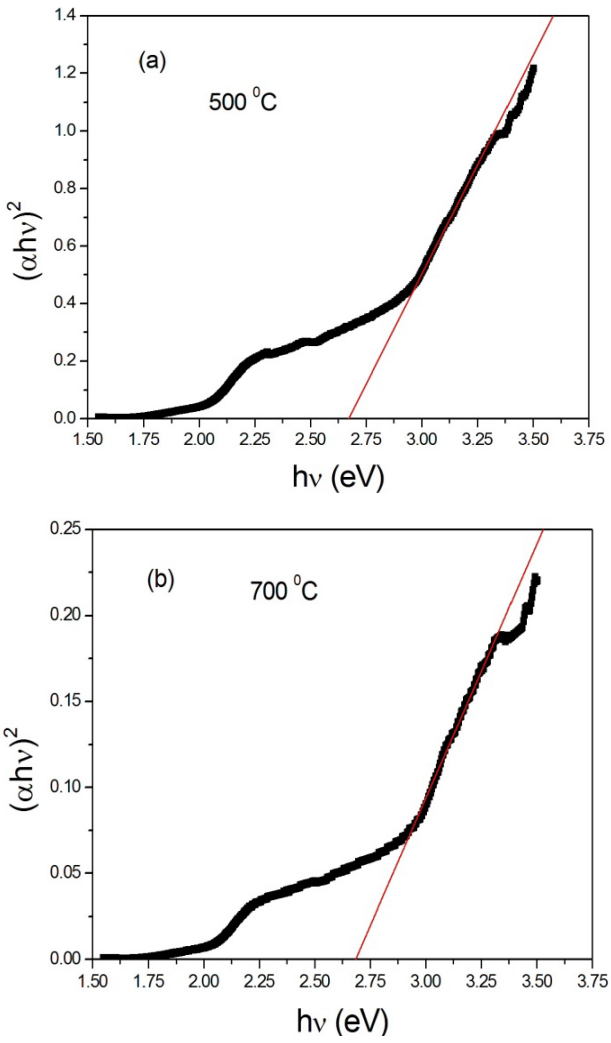

Figure 4. Variation of $(\alpha h\nu)^2$ vs. photon energy, $h\nu$ for α -Fe_2O_3 nanoparticles annealed at (a) 500 ℃ and (b) 700 ℃

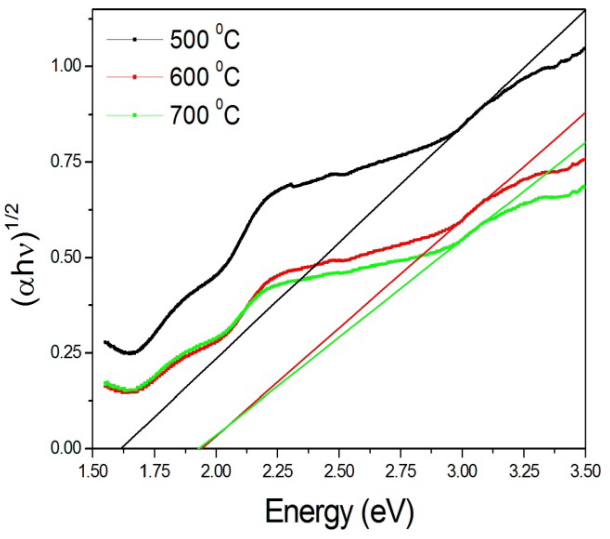

Figure 5. Variation of $(\alpha h\nu)^{1/2}$ vs. photon energy, $h\nu$ for α -Fe_2O_3 nanoparticles annealed at different temperatures

4. Conclusions

We report the effect of thermal annealing on the microstructure, optical absorption properties of hematite nanoparticles synthesized by low cost chemical route. Crystallite size and strain present in the sample increased and decreased respectively with increasing the annealing temperature. UV-visible optical characterization of these samples indicated the existence of both direct band gap and indirect band gaps. The value of direct band gap for the sample annealed at all temperatures estimated to be ~ 2.67 eV. The indirect band gap on the other hand increased from 1.6 to 1.94 eV when the annealing temperature increased from 500 to 600℃ and remained almost same for sample annealed at 700℃. The observed values of optical band gaps were in close agreement with the reported values. Our results indicated that the thermal annealing would give rise to well crystalline α-Fe_2O_3 nanoparticles with reduced strain.

ACKNOWLEDGEMENTS

The authors thank to Prof. N.C. Mishra, Utkal University, Bhubaneswar for his encouragement and also for providing Laboratory facility to carry out this work. DST, Govt. of India is acknowledged for proving XRD facility at Utkal University, Bhubaneswar under FIST programme.

REFERENCES

[1] N. Beermann, L. Vayssieres, S.-E. Lindquist and A. Hagfeldt, J Electrochem Soc 147, 2456 (2000).

[2] M.F. Al-Kuhaili, M. Saleem and S.M.A. Durrani, J Alloys Comp 521, 178 (2012).

[3] R. Zboril, M. Mashlan and D. Petridis, Chem Mater 14, 969 (2002).

[4] T. Almeida, Ph.D. Thesis. The University of Nottingham, 2010.

[5] I. Cesar, A. Kay , J.A. Gonzalez Martinez and M. Grätzel, J Am Chem Soc 128, 4582 (2006).

[6] T. Ohmori, H. Takahashi, H. Mametsuka and E. Suzuki, Phys Chem Chem Phys 2, 3519 (2000).

[7] X. Gou, G. Wang, J. Park, H. Liu and J. Yang, Nanotechnol 19, 125606 (2008).

[8] H. Zhou and S.S. Wong, ACS Nano 2, 944 (2008).

[9] D. Zitoun, N. Pinna, N. Frolet and C. Belin, J Am ChemSoc 127, 15034 (2005).

[10] C.Z. Wu, P. Yin, X. Zhu, C.Z. OuYang and Y. Xie, J Phys Chem B 110, 17806 (2006).

[11] K.J. Widder, A.E. Senyei and D.G. Scarpelli, Proceedings of the Society for Experimental Biology and Medicine 58, 141 (1978).

[12] G. Garcon, S. Garry, P. Gosset, F. Zerimech, A. Martin, M. Hannothiaux, et al., Cancer Lett 167, 7 (2001).

[13] R. Lawaczeck, M. Menzel and H.V. Pietsch, Appl Organometal Chem 18, 506 (2004).

[14] D. Walter, Thermochimica Acta 445, 195 (2006).

[15] M. Busch, M. Gruyters and H. Winter, Surf Sci 600, 4166 (2006).

[16] K. Woo, H.J. Lee, J.-P. Ahn and Y.S. Park, Adv Mater 15, 1761(2003).

[17] A. Glisenti, J Chem Soc Faraday Trans 94, 3671 (1998).

[18] P. Ayyub, M. Multani, M. Barma, V.R. Palkar and R. Vijayaraghavan, J Phys C: Solid State Phys 21, 2229 (1988).

[19] K. Cheng, Y.P. He, Y.M. Miao, B.S. Zou, Y.G. Wang, T.H. Wang, et al., J Phys Chem B 110, 7259 (2006).

[20] S. Giri, S. Samanta, S. Maji, S. Ganguli and A. Bhaumik, J Magn Magn Mater 285, 296 (2005).

[21] J. Lian, X. Duan, J. Ma, P. Peng, T. Kim and W. Zheng, ACS Nano 3, 3749 (2009).

[22] A. Askarinejad, M. Bagherzadeh and A. Morsali, J Experimental Nanosci 6, 217 (2011).

[23] P. Dhiman, A. Kumar and M. Singh, Adv Mat Lett 3, 330 (2012).

[24] O.M. Lemine, M. Sajieddine, M. Bououdina, R. Msalam, S. Mufti and A. Alyamani, J Alloys Comp 502, 279 (2010).

[25] G. Gordillo, J.M. Florez and L.C. Hernandez, Sol Energy Mater Sol Cells 37, 273 (1995).

[26] A. Banerjee, S. Patra, M. Chakrabarti, D. Sanyal, M. Pal and S.K. Pradhan, ISRN Ceramics 2011, Article ID 406094: doi:10.5402/2011/406094.

[27] D.A. Wheeler, G. Wang, Y. Ling, Y. Li and J.Z. Zhang, Energy Environ Sci 5, 6682 (2012) and references therein.

[28] Y.P. He, Y.M. Miao, C.R. Li, S.Q. Wang, L. Cao, S.S. Xie et al., Phys. Rev. B 71, 125411 (2005).

[29] T. Hashimoto, T. Yamada and T. Yoko, J Appl Phys 80, 3184 (1996).

[30] C.J. Sartoretti, B.D. Alexander, R. Solarska, I.A. Rutkowska, J. Augustynski and R. Cerny, J Phys Chem B 109, 13685 (2005).

[31] D.M. Sherman and T.D. Waite, Am Mineral 70, 11 (1985).

[32] N.F. Mott and E.A. Davies, Electronic processes in non-crystalline materials (Clarendon Press, Oxford,1979).

[33] A.N. Banerjee and K.K. Chattopadhyay, in DeplaD, Maheiu S (Eds.), Reactive sputter deposition (Springer-Verlag Berlin Heidelberg, 2008, p.465).

[34] N. Ozer and F. Tepehan, Sol Energy Mater Sol Cells 56, 141 (1999).

[35] G. Zotti, G. Schiavon and U. Casellato, J Electrochem Soc

145, 385 (1998).

[36] M. Gartner, M. Crisan, A. Jitianu, R. Scurtu, R. Gavrila, I. Oprea et al., J Sol–Gel Sci Technol 26, 745 (2003).

[37] A.A. Akl, Appl Surf Sci 233, 307 (2004).

[38] L. Dghoughi, B. Elidrissi, C. Bernede, M. Addou, M.A. Lamrani, M. Regragui et al., Appl Surf Sci 253, 1823 (2006).

[39] A. Duret and M. Gratzel, J PhysChem B 109, 17184 (2005).

[40] F.L. Souza, K.P. Lopes, P.A.P. Nascente and E.R. Leite, Sol Energy Mater Sol Cells 93, 362 (2009).

[41] E.L. Miller, D. Paluselli, B. Marsen and R.E. Rocheleau, Thin Solid Films 466, 307 (2004).